



# Physical factors controlling the diverse seismogenic behavior of fluid injections in Western Canada



Bei Wang<sup>a,b,\*</sup>, Honn Kao<sup>a,b</sup>, Hongyu Yu<sup>b</sup>, Ryan Visser<sup>b,d</sup>, Stuart Venables<sup>c</sup>

<sup>a</sup> School of Earth and Ocean Sciences, University of Victoria, Victoria, British Columbia, Canada

<sup>b</sup> Pacific Geoscience Centre, Geological Survey of Canada, Sidney, British Columbia, Canada

<sup>c</sup> British Columbia Oil and Gas Commission, Victoria, British Columbia, Canada

<sup>d</sup> Geoscience BC, Vancouver, British Columbia, Canada

## ARTICLE INFO

### Article history:

Received 19 August 2021

Received in revised form 30 March 2022

Accepted 15 April 2022

Available online xxxx

Editor: J.-P. Avouac

### Keywords:

induced seismicity

hydraulic fracturing

seismogenic potential

regional geological structure

stratigraphic setting

## ABSTRACT

Many factors, both natural and anthropogenic, can influence the seismogenic pattern of injection-induced earthquakes (IIE). With an enhanced earthquake catalog and a comprehensive fluid injection database compiled for the southern Montney play in northeast British Columbia, we explore the relative significance of the potential controlling factors of IIE. We first show that hydraulic fracturing (HF) operations are most likely responsible for the increased seismicity in the region. For areas with comparable HF activities, the regional structural geology could be one primary factor correlating with the distribution of IIE. Our investigations further reveal that the stratigraphic formation for HF is the next important factor deciding the level of IIE. Specifically, the number of HF stages targeting the Upper Montney is about five times of that targeting the Lower-Middle Montney (LMM), yet the latter ones are responsible for the majority of IIE. The elevated seismic response with LMM may be attributed to two possible mechanisms, 1) the proximity to deeper permeable formations and subvertical graben faults that facilitates the downward migration of injected fluid and stress perturbation to reactivate pre-existing faults in the basement, and 2) the geomechanical heterogeneity of the two newly recognized geological units (Altares Member and Pocketknife Member) along the upper and lower boundaries of the LMM that enhances the seismogenesis of IIE. Our results provide an important framework of constructively mitigating the injection-related seismic hazard.

Crown Copyright © 2022 Published by Elsevier B.V. All rights reserved.

## 1. Introduction

Induced earthquakes are defined as events caused by anthropogenic activities, and their occurrence can be traced back over five decades (Healy et al., 1968; Raleigh et al., 1976). During the past 10 years, subsurface fluid injection has drawn increasing attention due to the association with a dramatic increase in regional/local seismicity. For example, the number of earthquakes with magnitude larger than 3 increased by a factor of 10 in the central U.S. Most of these events have been attributed to wastewater disposal (WD) operations that are often associated with high injection rates and a large amount of cumulative volume (Ellsworth, 2013; Keranen and Weingarten, 2018). Comparably, hydraulic fracturing (HF) stimulations can also trigger M4+ earthquakes, and many cases have been documented in the West-

ern Canada Sedimentary Basin (WCSB) and southwest China (e.g., Atkinson et al., 2016; Bao and Eaton, 2016; Lei et al., 2019; Schultz et al., 2018; Wang et al., 2020).

Progress has been made to characterize the various controlling factors of the HF-related injection-induced earthquakes (IIE) in WCSB. For example, Schultz and Eaton (2018) suggested that IIE preferentially locate within regions with overpressured formations, while Schultz et al. (2016) and Galloway et al. (2018) found that specific geological conditions, such as the reef margins and fault-related karst feature, tend to correlate with more IIE due to their ability of guiding fluid flow to the faults. Similarly, Wang et al. (2020) and Peña Castro et al. (2020) proposed that several of the largest IIE in western Canada have occurred on pre-existing faults with possible direct connection to high-permeable conduit structures. Schultz et al. (2018) further delineated a linear relationship between the cumulative injection volume of a single pad and the number of HF-related IIE. Many studies also suggested that the in-situ regional stress could be another important factor facilitating seismic slip on a fault (e.g., Shen et al., 2019; Zoback and Lund Snee, 2018). On a regional scale, Kao et al. (2018) pointed out that

\* Corresponding author at: Pacific Geoscience Centre, Geological Survey of Canada, Sidney, British Columbia, Canada.

E-mail address: beiwang@uvic.ca (B. Wang).

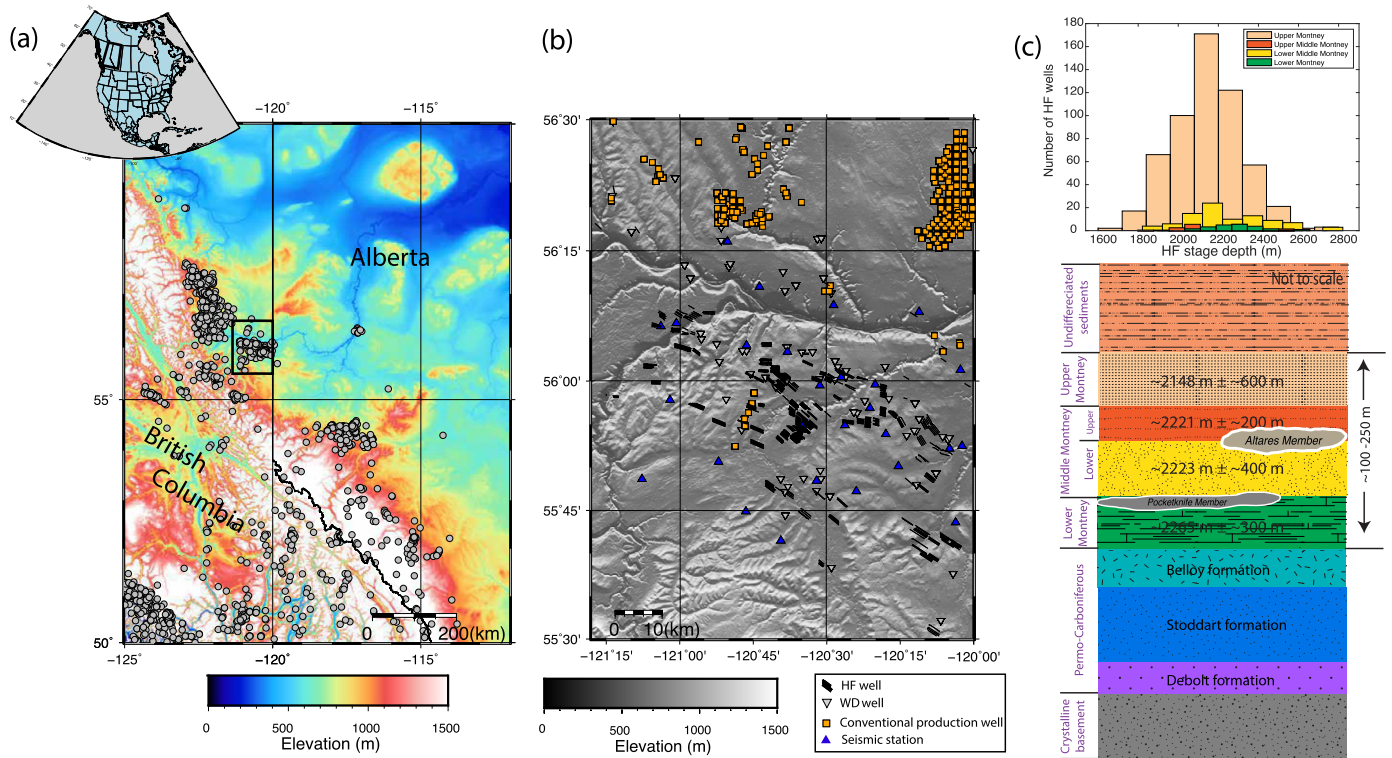


**Fig. 1.** Spatial distribution of earthquakes and injection wells in western Canada. (a) Grey circles mark epicenters of M3+ seismicity in northeastern British Columbia and western Alberta between 2011 and 2020 as reported by Natural Resources Canada. The black rectangle marks the study area. (b) Seismic stations, conventional oil-and-gas production wells, hydraulic fracturing (HF) wells and wastewater disposal (WD) wells in the study area. (c) The top panel shows the numbers of HF wells targeting different Montney formations as a function of depth. The bottom panel is a schematic diagram of the stratigraphic units describing the geological context of the Montney formations. (For interpretation of the colors in the figure(s), the reader is referred to the web version of this article.)

the tectonic strain rate plays a key role in controlling the spatial distribution of IIE in the WCSB.

These observations provide a first order understanding of the seismogenic factors of IIE in the WCSB. However, comprehensive investigations to evaluate their significance among these factors are hindered by the lack of high-quality IIE catalog and the incomplete access to well operation database. In addition to delineating possible controlling factors of IIE in western Canada, there are two key conundrums on their causal mechanisms. One is why the seismic response to comparable injection activities within the same shale play varies significantly. An interesting example is the Duvernay play in Alberta where the Kaybob region is more seismogenic than the Willesden Green and Edson regions (Schultz et al., 2018). Another one is how to forecast the corresponding seismogenic behavior when multiple formations are targeted by the same hydraulic fracturing (HF) pad. One typical example is the southern Montney play (SMP) in northeast British Columbia where the stratigraphy can be subdivided from top to bottom into the Upper Montney (UM), Upper Middle Montney, Lower Middle Montney (LMM) and Lower Montney (Davies et al., 2018) (Fig. 1). The HF operations targeting these formations present a natural laboratory to differentiate the possible seismic response within different stratigraphy.

Recently, the seismic station coverage in northeast British Columbia has been systematically improved since 2013 (Fig. 1). The newly established stations have lowered the regional earthquake detection threshold by at least one magnitude unit (Mahani et al., 2016), and thus provide us a unique opportunity to investigate the detailed spatiotemporal distribution of IIE with respect to potential influencing factors at an unprecedented resolution. In this study, we conduct a series of Monte Carlo tests and detailed statistical analysis with the enhanced catalog to determine the

relative significance of physical factors that control the local seismogenic pattern of IIE. We propose a schematic model with the injection type, regional structural geology, and the stratigraphic setting being the most influential factors to explain our observations. For the first time, we find that injections, even at the same geographic location, can have very different IIE responses depending on the target's stratigraphic setting. This finding will help bridge the gap in our understanding of how anthropogenic/hydrogeologic/stratigraphic factors affect the occurrences of IIE, and lead to a substantial progress in an effective mitigation of injection-related seismic hazard.

## 2. Data and methods

We compile the fluid injection parameters from completion reports in the BC Oil and Gas Commission database (<https://www.bcogc.ca/>, last accessed 07 July 2021). The WD injection is usually a continuous process lasting for months, in contrast to a HF stage that is often finished within a few hours. There is also a big difference in the injection rate ( $\sim 0.5$  m<sup>3</sup>/min of WD injections vs.  $\sim 10$  m<sup>3</sup>/min of HF). In this study, we quantify the WD and HF injection operations in the unit of month and stage, respectively, based on the technical/completion reports submitted to the regulator by local operators. In total, there are 20293 HF stages at 778 horizontal wells and 1151 WD injection months at 58 active WD wells.

We use waveform data from broadband seismic stations belonging to three local and regional seismograph networks (network codes XL, 1E, and PQ, operated with a digitization rate of 100 samples per second). We first deploy the sophisticated earthquake location method "Source-Scanning based on Navigated Automatic Phase-picking" (Tan et al., 2019) to detect and locate events within our study area between 1 January 2017 and 31 December 2018 (details are given in Supplement Note 1). To minimize

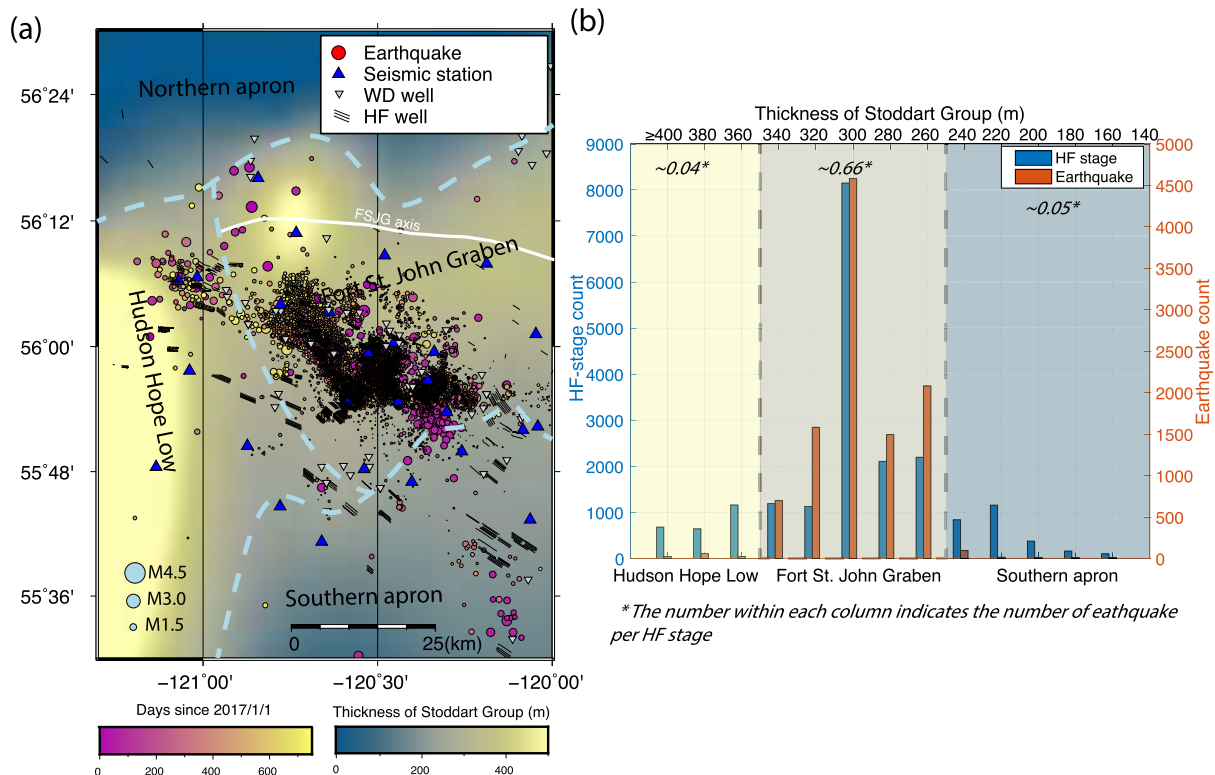


**Fig. 2.** Major geological structures and the seismic pattern in our study area. (a) Spatiotemporal distribution of IIE with respect to the regional structural geology. Thick dashed lines represent the inferred boundaries of different tectonic elements based on the thickness of the Stoddart Group. White line marks the FSJG axis adopted from O'Connell et al. (1994), and the boundary between FSJG and HHL may vary. (b) Numbers of HF stages and earthquakes corresponding to different Stoddart Group thickness. Note that the Stoddart Group thickness of each earthquake is approximated with the measurement at the closest HF well.

errors from inaccurate travel times, we adopt the 1-D velocity model developed particularly for the SMP area by Babaie Mahani et al. (2020). About 250 times more events have been detected and located (10693 events in total, as shown in Fig. 2a), compared to the routine earthquake catalog reported by Natural Resources Canada. As shown in Fig. S1, the magnitude-frequency distribution suggests that the magnitude of completeness for the enhanced catalog is  $\sim 1$  and the corresponding  $b$ -value is  $0.93 \pm 0.01$  based on the maximum-likelihood estimation (Aki, 1965; Wiemer and Wyss, 2000).

Next, we use the newly developed Depth-Scanning Algorithm method (Yuan et al., 2020) to refine the focal depth of earthquakes with  $M > 2.5$  in the enhanced cataloged. This technique improves the focal depth accuracy by incorporating the travel time constraint from depth phases recorded at local and regional distances. Here, we set the scanning range of focal depth from 1 to 35 km. There are 3 major steps in the scanning process. First, the waveforms of all possible depth phases are constructed from the direct P and S phases. Second, the synthetic depth-phase waveforms are used as templates to scan the observed seismograms for any segments with high waveform similarity. Finally, the depth corresponding to the largest number of depth-phase matches and minimum accumulated travel time residual is deemed the final solution (more details are given in Supplement Note 2).

With the enhanced earthquake catalog and compiled fluid injected data, we conduct two Monte Carlo tests to verify whether IIE are statistically correlated with injection activities. In the first test, we create 10,000 synthetic catalogs (each with the same number of events as the real catalog) based on the naïve assumption of all epicentral distributions being random following the method of Schultz et al. (2016). In the second test, we also create 10,000 synthetic catalogs, but assume that the distribution of earthquakes is constrained by the location of fault systems (i.e., earthquakes

should occur within 1 km from faults). For each synthetic catalog, we calculate the average distance between earthquake epicenters and their nearest injection activities. These 10,000 averaged event-well distance values from synthetic catalogs are compared with the actual distances derived from the real catalog and injection data.

Finally, we deploy a spatiotemporal correlation filter to associate IIE with corresponding HF stages to determine the role of stratigraphic setting, similar to prior studies (Schultz et al., 2018). We first require the earthquake to occur within a certain time window after the stimulation stage. Once the temporal criterion is satisfied, we assign this earthquake to the nearest HF stage if the pair satisfies the spatial criterion (more details in Supplement Note 3). Detailed information on the stratigraphic setting of all injection wells is retrieved from the BC Oil and Gas Commission database (<https://www.bcogc.ca/>, last accessed 07 July 2021).

### 3. Results

In this section, we systematically delineate the physical factors that control the IIE pattern of the SMP. We first focus on the large-scale relationship between local seismicity and injection operations regardless of the regional geological setting. After recognizing the HF stimulation as the first influential factor, we narrow down to a smaller scale to examine if regional geological structures could affect the triggering capacity of HF-related IIE. Finally, within the same geological setting, we zoom in further to the stratigraphic scale to explore the variation of triggering capacity when different formations are targeted.

#### 3.1. First influential factor: type of injection

As shown in Fig. S3 and S4, our two Monte Carlo test results suggest that the synthetic earthquake catalogs all have significantly

greater event-well distances when compared to the original catalog ( $\sim 10/\sim 8$  km vs.  $\sim 1$  km for catalogs with earthquakes randomly distributed and catalogs with earthquake epicenters constrained by faults, respectively). Since none of the 10,000 synthetic catalogs yields the averaged event-well distance comparable to the observed value, the probability of earthquakes being randomly distributed in our study area must be  $<10^{-4}$ . This result implies that the association between earthquakes and injection operations is statistically significant.

We then calculate the average distance between individual cataloged earthquakes and their nearest HF and WD wells, following the same approach used in a previous study (Schultz et al., 2018). We find that the average distance from an earthquake epicenter to the closest WD operation is  $\sim 4$  times of that to the closest HF stage ( $\sim 4$  km vs.  $\sim 1$  km, Fig. S5). Meanwhile, 94% of all observed earthquakes are closer to HF than WD wells. Both results suggest that HF activities might play a more important role on inducing local seismic events. To ensure that the closer average distance between HF and IIE is not a bias from the difference between the large number of HF stages and the relatively fewer WD operation months, we repeat the Monte Carlo test by generating 10,000 HF stage lists (each with 1151 samples, the same number of WD operation months, randomly selected from the original HF database). As shown in Fig. S6, the result suggests that the average distance from an IIE epicenter to the nearest HF activity is still much smaller than that to the nearest WD activity ( $\sim 1.2$  km vs. 4.2 km).

We note that simply using the event-well distance to distinguish the relative influence of different injection types can be ambiguous. To further verify the statistical significance of the relationship between injection types and seismicity, we conduct one additional Monte Carlo test to examine the temporal correlation (e.g., Savvaidis et al., 2020). Our null hypothesis is that the earthquakes are not induced by HF stimulations, thus no temporal correlation between HF stages and IIE is expected. Specifically, we create 1000 synthetic catalogs from the real one. While the hypocenters are kept unchanged for each synthetic catalog, the origin time of each event is randomly picked between 1 January 2017 and 31 December 2018. We then calculate the delay time between each event and the start of the injection at the closest well stage within a prescribed distance range (1 km, 3 km, and 5 km). In Fig. S7, we show the distributions of injection-event delay time for the real catalog and one representative synthetic catalog. While most of the events in the real catalog have injection-event times of 3 days or less (Fig. S7a), the synthetic catalog appears to have a much more uniform distribution up to 30 days (Fig. S7b). Taken the entire set of 1000 synthetic catalog together, the mean value of the injection-event delay time of each synthetic catalog falls mainly in the range of 14–16 days (Fig. S7c). This is in sharp contrast to the much shorter average delay time of only  $\sim 6$  days for the real catalog. Our Monte Carlo test results clearly suggest that the null hypothesis of no temporal correlation between HF and IIE can be rejected at the confidence level of over 99% ( $p < 0.01$ ).

### 3.2. Second influential factor: regional structural geology

In our study area, the predominant geological structure is the Dawson Creek Graben Complex, consisting of the core Fort St. John Graben (FSJG), the western zone of greater subsidence (i.e., the Hudson Hope Low, HHL), the northern and southern sediment aprons, and the satellite smaller grabens to the east (Barclay et al., 1990; O'Connell et al., 1994). The structural development of the Dawson Creek Graben Complex is closely linked to the deposition of the Stoddart Group and the thin overlying Belloy formation (Barclay et al., 1990). Barclay et al. (1990) use the thickness of the Stoddart Group as a proxy to estimate the boundary of the FSJG, which is an asymmetrical structure with a gently sloping, but

less constrained, southern apron. Conventionally, different thickness contours of the Stoddart Group are used to define the northern and southern edges of the FSJG (ranging from  $\sim 140$  to  $\sim 430$  m). For the sake of making quantitative analysis and fair comparison, we take a more consistent approach in this study by using the median value of 250 m of the Stoddart Group thickness to define the boundaries between the FSJG and the surrounding aprons. The boundary between the FSJG and the deeper HHL to the west is adopted from O'Connell et al. (1994) (Fig. 2a).

We count the number of earthquakes spatially correlated with the HF stages within the areas of FSJG, HHL, and the southern apron (the number of HF wells in the northern apron is inadequate). As shown in Fig. 2, the level of seismicity is the highest within the FSJG area (corresponding to the Stoddart Group thickness between 250 and 350 m), whereas the number of earthquakes is almost negligible in areas of HHL and the southern apron. Particularly, we observe 9812, 103, and 135 events for FSJG, HHL and southern apron, respectively, while the corresponding numbers of HF stages performed in these three areas are 14778, 2488, and 2642. On average, the ratio between the numbers of earthquakes and HF stages is  $\sim 0.66$  in the FSJG area, but only  $\sim 0.041$  and  $\sim 0.051$  in the areas of HHL and the southern apron. These results suggest that HF injections in the FSJG area have a much higher chance to induce an earthquake.

Next, we examine whether the drastic different levels of local seismicity can be explained by different cumulative volumes of injected fluids. It turns out that the cumulative injected volume is approximately linearly correlated with the cumulative number of HF stages (Fig. S8). Subsequently, the total volume of HF injections in the FSJG area is approximately  $\sim 5.9$  times of that in the HHL area, and  $\sim 5.6$  times of that in the southern apron. The number of earthquakes per one million cubic meters of injected volume is  $\sim 1328$  for FSJG area, around 15 times of that in the HHL area ( $\sim 83$ ) and southern apron ( $\sim 102$ ). That is, the difference of injection volumes cannot fully address the extreme variations between local seismicity in the three subareas, these ratios again underscore the significance of the area's geological structures.

### 3.3. Third influential factor: stratigraphic setting

In the SMP, the majority of HF stimulations aim at the UM, followed by the LMM, and only a very small number of HF wells target the Upper Middle Montney and Lower Montney (Fig. 1c). The depth range of each Montney formation can vary from one location to another, ranging from  $\sim 1.5$  km to  $\sim 2.5$  km below the surface as inferred from HF completion reports. Overall, the total thickness of the Montney formation is  $\sim 100$ – $250$  m. The seismic response to injections at different formations (or depths) remains unclear.

Here, we focus solely on the HF-related IIE within FSJG to avoid any bias from different injection types (i.e., the first influential factor) and regional structural geology (the second influential factor). Fig. 3 shows the results of our spatiotemporal correlation filter analysis using time and distance thresholds of 3 days and 3 km, respectively. Results for other combinations of spatiotemporal criteria are presented in Fig. S9. While the number of HF stages targeting the LMM is only  $\sim 1/5$  of that targeting the UM, the number of IIE associated with the LMM HF stimulations is much higher (Fig. 3b and S9). We obtain similar results when we apply the same spatiotemporal correlation filter analysis with a higher magnitude threshold (Fig. S10). Furthermore, we conduct the  $p$ -test to examine the validity of a null hypothesis that HF stages targeting the UM and LMM have the same earthquake triggering capacity (see Supplement Note 4 for details). The numbers of earthquakes predicted by this hypothesis (solid black lines, Fig. 3c) are completely inconsistent with our observations (pink and blue lines, Fig. 3c),

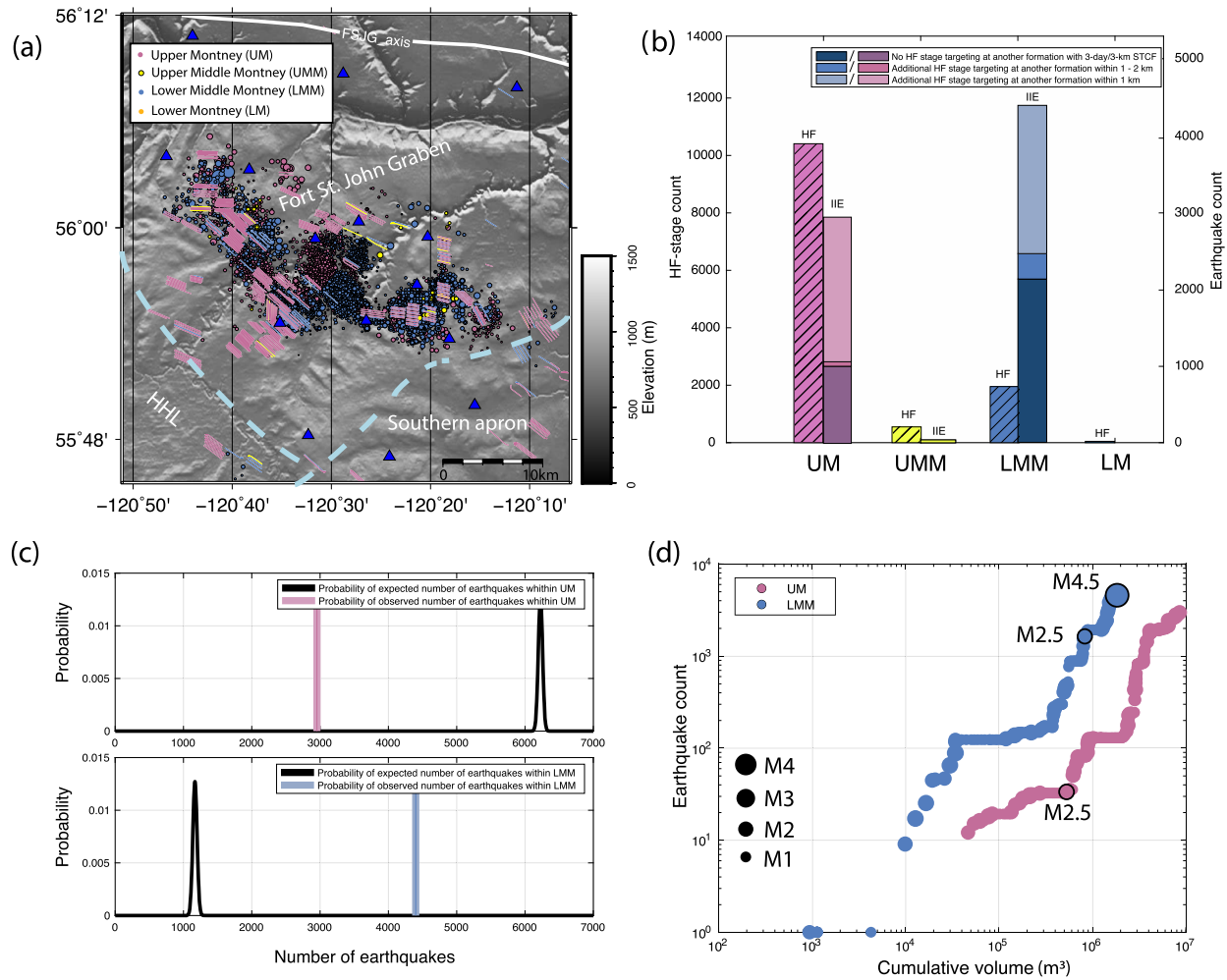


**Fig. 3.** Statistical results after applying a 3-day/3-km spatiotemporal correlation filter. (a) Spatial distributions of epicenters (circles) and surface projections of horizontal HF wells (thin lines) associated with injections into different Montney formations. (b) Histograms showing the numbers of HF stages and earthquakes associated with each Montney formation. The confidence in the correlation between HF stage and earthquake is expressed as the tone of the color (darker means higher confidence, see Supplement Note 3 for details) (c) Probability as a function of the designated number of earthquakes associated with HF (thick black line) in the UM (top panel) and LMM (bottom panel), assuming that earthquakes can be equally triggered by HF stages regardless of their targeted formations. Colored vertical lines mark the observed numbers of earthquakes. (d) Number of earthquakes as a function of the cumulative injected volume for the UM and LMM. The size of circles corresponds to the maximum magnitude within the same volume interval.

implying that the null hypothesis can be statistically rejected at the confidence level of over 99% ( $p < 0.01$ ).

Finally, to quantitatively characterize the different seismic responses of the UM and LMM, we compile the volumes used in individual HF stages and the number of IIE for the two formations separately, and the result is shown in Fig. 3d. It is interesting to note that the two lines are similar except the UM has approximately an order more cumulative volume, given the same IIE count. This difference suggests that the triggering capacity of IIE in the LMM is probably one order higher than that in the UM.

### 3.4. Other operational factors

In addition to the injected volume, we also investigate if other operational parameters could contribute to the discrepancy of IIE triggering capacity among the three areas, including the breakdown pressure, injection rate, shut in pressure, and average treating pressure. We find that all these operational parameters appear to have comparable values without distinctly following the IIE distribution pattern (Fig. S11). Therefore, the difference is not large enough to justify the dramatic difference in the observed seismic pattern.

## 4. Interpretation

After delineating the controlling factors associated with deep fluid injection, we propose a schematic model to interpret our findings. Fig. 4 is a schematic diagram to summarize our model. The first controlling factor is the injection type. As shown in Fig. S5 – S7 and suggested by the results of our Monte Carlo tests, the vast majority of IIE in the SMP are associated with HF injections (>80% with 3 day/3 km spatiotemporal correlation filter, also suggested by Dokht et al. (2021)). The next important controlling factor is the regional structural geology. Specifically, HF-related IIE are more likely to occur if stimulations are performed in the FSJG area than in the neighboring HHL and southern apron areas. Then, the third controlling factor is the stratigraphic setting. Once inside the FSJG area, we find that HF stages targeting the LMM statistically cause more IIE than those targeting other formations, even though the corresponding cumulative injected volume is only one fifth.

Our finding that HF stimulations are associated with many more IIE than WD injections in our study area is not a surprise, as similar conclusion has been reported by previous studies (Atkinson et al., 2016; Schultz and Eaton, 2018; Wang et al., 2021; Yu et al., 2020). However, we would like to point out that the interpretation

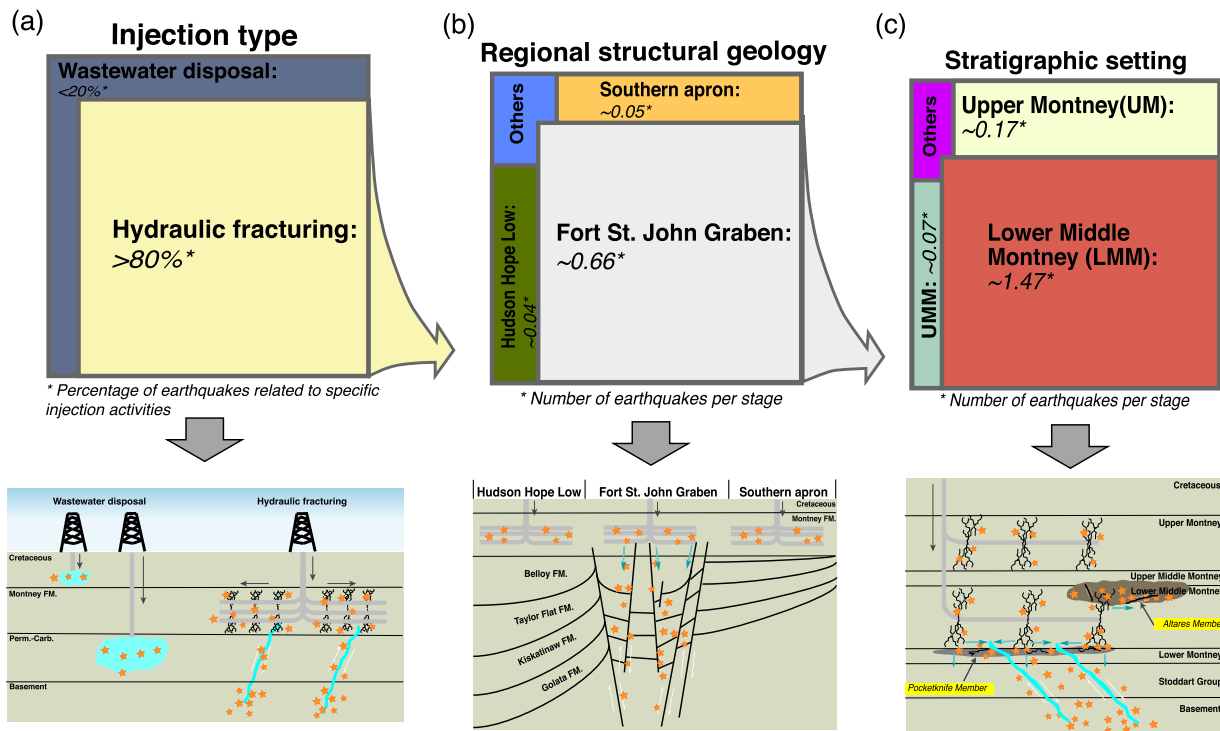


**Fig. 4.** A schematic diagram showing the three important physical factors controlling the IIE in the southern Montney Play. The bottom sketches illustrate the corresponding seismogenic mechanisms of IIE for the top three factors. (a) Injection type is the first important factor. More than 80% of all IIE (orange stars, with a 3-day/3-km spatiotemporal correlation criterion) are related to hydraulic fracturing (HF), and can occur in the vicinity of injection depth and the basement via hydraulic conduits. (b) Regional structural geology is the second important factor. The number of earthquakes per HF stage is the highest within the area of FSJG filled with subvertical faults. The blue arrows show the potential fluid migration along the graben faults. (c) Stratigraphic setting is the third important factor. The numbers of earthquakes per HF stage is the highest when the LMM is the HF target. The higher IIE rate may be related to the presence of the Altares Member and Pocketknife Member along the top and bottom sections of the LMM, respectively. Horizontal blue arrows show the fluid migration along the bedding contacts and possibly intersecting with graben faults, while the small vertical blue arrows show the slow diffusion via the permeable Permo-Carboniferous formations below the LMM.

of this observation should be exercised with caution. A direct communication with the regulator confirms that the location of all WD wells in northeast British Columbia were carefully selected to minimize the chance of causing IIE. Specifically, they avoid any known fault structures, and target reservoirs that are less communicable to surrounding formations with confining layers. Thus, the diverse seismic responses to HF and WD may be, at least in part, a consequence of the industry's own mitigation practice in the SMP.

The higher number of HF-related IIE in the FSJG area than the surrounding HHL and apron areas may be explained by the unique geological characteristics. First, the FSJG has been intensely segmented and faulted in blocks during the sedimentary subsidence (Barclay et al., 1990). A recent study based on the spatiotemporal distribution of HF-related IIE and high-resolution 3-D seismic images near Fort St. John reveals multiple buried thrust faults extending from the basement up to the Montney formation and a pervasive system of transverse structures (Riazi and Eaton, 2020). These thrust and transverse faults could act as potential pathways for aseismic pore-pressure diffusion to migrate farther that, in turn, increase the possibility of causing more IIE in the vicinity (e.g., Eyre et al., 2019; Galloway et al., 2018; Lei et al., 2017; Peña Castro et al., 2020; Schultz et al., 2016; Wang et al., 2021; Yu et al., 2021a). Moreover, one of the largest fault systems in the region, the Gordondale Fault, runs subparallel to the axis of the FSJG and extends eastward to central Alberta (Eaton et al., 1999). It could also contribute to the higher IIE potential in the FSJG area. It is worth noting that the difference in the rate of seismicity among the three subareas cannot be an artifact due to network coverage, as the detection threshold (i.e., the magnitude of completeness) is almost the same (Fig. S12).

The more active seismogenic behavior of the LMM than UM could be related to its deeper depth and unique stratigraphic setting. First, many previous studies suggest that larger IIE earthquake sequences tend to nucleate on pre-existing faults located in the deeper crystalline basement that are reactivated by fluid injections (e.g., Bao and Eaton, 2016; Lei et al., 2017, 2019; Riazi and Eaton, 2020; Schultz et al., 2016; Skoumal et al., 2018; Wang et al., 2020). In our study area, the recalibrated focal depths of the two largest IIE (M4.5 on 30/11/2018 and M3.3 on 30/11/2018) are also located deeper than the Montney formation at ~2.6 and ~3.9 km, respectively, likely in the Stoddart Group or in the basement (Fig. S2). More importantly, there are two newly recognized groups of bioclastic beds, named as the Altares Member and Pocketknife Member, intercepting and interfingering with the LMM at the top and bottom sections, respectively (Fig. 1c and 4c) (Zonneveld and Moslow, 2018). Both members have distinctly low content of total organic carbon and high proportion of recrystallized skeletal calcite from shell materials. As faults with calcite gouge generally have higher shear strength than that with clayey gouge (Ikari et al., 2013; Verberne et al., 2014), it is conceivable that deformation caused by fluid injection within the LMM interfingering with the Altares Member/Pocketknife Member is more likely to be released as brittle failures. This argument is consistent with the pervasive faulting and fracturing/slickenside structures observed within the core samples of Altares Member (Sanders et al., 2018), and compatible with recently reported upward seismicity migration pattern from the target formation (Peña Castro et al., 2020; Schultz and Wang, 2020). In contrast, the higher content of clay and total organic carbon in the UM may favor stable sliding that release the injection-related deformation as aseismic slip (Eyre et al., 2019).

## 5. Discussion

The volume of injected fluid has been regarded as one of the key controlling factors in inducing earthquakes within the WCSB. For example, Farahbod et al. (2015) found that in the Horn River Basin, northeast British Columbia, Canada, the number of IIE started to surge after the monthly cumulative HF injection volume (summed over the entire basin) exceeded the level of  $2.0 \times 10^4 \text{ m}^3$ . Yu et al. (2021b) documented a sharp increase of IIE in a local area of west Alberta, Canada, following 25 years of continuous WD injection. With more data from the Fox Creek area, Schultz et al. (2018) suggested that the cumulative injected volume per each injection pad could be linearly related to the seismic productivity when it is on the order of  $10^4$ – $10^5 \text{ m}^3$ . In this study, we consider the cumulative injection volume as a necessary condition for the seismogenesis of IIE. While our observations in the SMP support the notion that cumulative volume is a key factor for IIE, the linear relationship between injected volume and the number of IIE derived for one place may not be applicable to others (Fig. 2 and Fig. S13). Instead, the FSJG area has a much higher IIE/HF-stage ratio ( $\sim 0.66$ ) than the two neighboring areas (0.041 and 0.051, Fig. 2b). Since the cumulative injected volume in the FSJG area is also the highest, it is likely that the pervasive fault system in the graben and the large cumulative volume both contribute positively to the higher seismicity. It is also worth mentioning that the comparison of cumulative volume between HF and WD injections are not considered in our spatiotemporal criteria. In order to clearly discriminate the roles of WD and HF injections on inducing specific IIE sequences, a quantitative analysis on the stress perturbation caused by these two types of injections is required, but is beyond the scope of this study.

For the cumulative volume to become an important controlling factor of IIE, our observations suggest that the cumulative injected volume must exceed a certain threshold before the wide-spread occurrence of IIE (Fig. 3d). Once the outbreak threshold is passed, the occurrence rate of IIE can significantly outpace the rate of volume increase. As more fluid is injected into the rock formations, it could lead to more deformation by the poroelastic effects, pore pressure diffusion to a broader region, and additional creep and aseismic slip along pre-existing faults that, in turn, cause additional stress perturbations and earthquakes (Deng et al., 2016; Eyre et al., 2019; Gao et al., 2022; Goebel et al., 2017; Segall and Lu, 2015; Wang et al., 2021; Yu et al., 2021a, 2019). The nonlinear relationship between the number of IIE and injected volume probably further hint the important role played by the regional/local geological structures.

Although we do not have the depth resolution to demonstrate that all IIE associated with HF targeting the LMM are deeper than those targeting the UM or Upper Middle Montney, results of our spatiotemporal correlation filter analysis clearly suggest that stimulating the relatively deeper LMM correlates with a higher rate of IIE (Fig. 3). We speculate that the relatively porous and permeable formations (Permo-Carboniferous) immediately beneath the Montney (i.e., the Belloy, Stoddart, and Debolt, Fig. 1c) may play an important role. Specifically, these formations have pervasive pre-existing faults, formed during the Paleozoic subsidence, that can be reactivated by injections to host IIE (Barclay et al., 1990; O'Connell et al., 1994). They can also act as effective conduits for the fluid and stress perturbation caused by injections to reach the deeper, and presumably more seismogenic, crystalline basement (Skoumal et al., 2018). Assuming that the geomechanical perturbation by each HF stage is comparable regardless of the targeted formation, the chance of causing IIE by HF stimulations to the LMM becomes higher due to its close proximity to the deeper Permo-Carboniferous formations and basement.

The sharp hydrological contrast between the LMM and Altares Member/ Pocketknife Member may also contribute to the higher seismogenic potential of the LMM, as the injected fluid can migrate more easily along the bedding contacts to a broader area (Sanders et al., 2018). Such horizontal migration may increase the chance for injected fluid to reach more subvertical faults within the FSJG, and potentially trigger more IIE in the basement (Fig. 4c). It is worthy pointing out that HF stimulations targeting the LMM within the HHL and southern aprons have caused considerably fewer IIE than those within the FSJG (Fig. S14). One interpretation could be that the total injected volume within HHL and southern aprons is below the threshold capable of causing wide-spread occurrence of IIE. Meanwhile, we cannot rule out the possibility that the interactions between the inferred horizontal migration (due to, e.g., the bedding contacts) and pervasive subvertical faults within the FSJG graben help to enhance the seismogenic potential of LMM.

Overall, the highly heterogeneous distribution of IIE in the SMP manifests the combined effects of different physical mechanisms. In case that one factor (e.g., HF stimulation) systematically interfere with the others (e.g., the geological structure of subvertical or décollement faults (Riazi and Eaton, 2020), the existence of stratigraphic members with distinct geomechanical/hydrological characteristics, and proximity to the crystalline basement), the likelihood of IIE occurrence becomes substantially higher (Fig. 4).

## 6. Conclusion

We investigate the spatiotemporal correlation between injection operations and regional seismicity in western Canada. We find  $\sim 80\%$  IIE are associated with HF stimulations in the SMP. By conducting Monte Carlo tests with synthetic earthquake catalogs, the hypothesis of regional seismicity being randomly distributed can be statistically rejected (probability  $< 10^{-4}$ ). We also find that HF stimulations performed in the FSJG area have a much higher chance to induce earthquakes than those in the surrounding areas ( $\sim 0.66$  vs.  $< 0.05$  event per HF stage). Given the same setting of structural geology and injected volume, the seismogenic response to HF stimulations could vary significantly when different formations are targeted. In the SMP, the number of HF stages targeting the LMM is only 1/5 of that targeting the UM, yet the number of corresponding IIE is actually higher ( $\sim 1.47$  vs.  $\sim 0.17$  event per HF stage).

Based on our observations, we propose a schematic model to interpret the diverse IIE patterns. The enhanced seismogenic potential of HF stimulations targeting the LMM could be explained by at least two reasons. First, the LMM is in proximity to deeper permeable formations and subvertical graben faults that may facilitate the downward migration of injected fluid. The associated stress perturbation due to elevated pore pressure could help reactivate pre-existing faults in the basement. Secondly, the geomechanical heterogeneity of two geological units (Altares Member and Pocketknife Member) along the upper and lower boundaries of the LMM may enhance the seismogenesis of local IIE. The lower content of total organic carbon, higher proportion of recrystallized calcite, and sharp hydrogeological contrast to the Montney formations probably collectively contribute to the inferred geomechanical heterogeneity.

A key implication of our study is that decisions on the geographic location of injection wells and their targeted formation(s) can lead to a big difference in the effectiveness of managing the seismic risk due to IIE. Therefore, HF stimulations targeting the formation with a higher IIE triggering capacity (e.g., the LMM in the FSJG area) should be closely monitored. On the other hand, formations without the characteristic conditions of IIE can probably sustain more HF stimulations and/or larger injected volumes under the same regulatory framework. This aspect should be prop-

erly considered in the design of HF stimulations to achieve the best balance between stimulation efficiency and seismic safety.

### CRediT authorship contribution statement

H.K., B.W., S.V. designed research; B.W., H.K., H.Y., R.V., and S.V. performed research; B.W., H.K., H.Y., and R.V. analyzed data; and B.W., H.K., H.Y., and S.V. wrote the paper.

### Declaration of competing interest

The authors declare that they have no known competing financial interests or personal relationships that could have appeared to influence the work reported in this paper.

### Acknowledgements

The NRCan earthquake catalog can be downloaded through the website, <http://www.earthquakescanada.nrcan.gc.ca/stndon/NEDB-BNDS/bulletin-en.php>. The enhanced earthquake catalog is available at <https://doi.org/10.5281/zenodo.5879921>. Seismic waveforms for NRCan stations are publicly available on the Incorporated Research Institutions for Seismology (IRIS) website (NBC4-5, NBC7-8, and MONT1-4, network code 1E and PQ), and waveforms for seismic stations operated by McGill University and Ruhr-University Bochum (MG01-09, RU01-06, IRIS network code XL, sampling rate: 100 Hz) are available on IRIS upon request. The injection well data can be accessed through BC Oil and Gas Commission website, <https://www.bcogc.ca/data-reports/data-centre/>. This study is partially supported by the Induced Seismicity Research Project of NRCan (HK), Geoscience BC (HK). This paper is NRCan contribution 20210700.

### Appendix A. Supplementary material

Supplementary material related to this article can be found online at <https://doi.org/10.1016/j.epsl.2022.117555>.

### References

Aki, K., 1965. Maximum likelihood estimate of  $b$  in the formula  $\log N = a - bM$  and its confidence limits. *Bull. Earthq. Res. Inst. Univ. Tokyo* 43, 237–239.

Atkinson, G.M., Eaton, D.W., Ghofrani, H., Walker, D., Cheadle, B., Schultz, R., Shcherbakov, R., Tiampo, K., Gu, J., Harrington, R.M., Liu, Y., van der Baan, M., Kao, H., 2016. Hydraulic fracturing and seismicity in the Western Canada sedimentary basin. *Seismol. Res. Lett.* 87, 631–647.

Babaie Mahani, A., Malyskiy, D., Visser, R., Hayes, M., Gaucher, M., Kao, H., 2020. Well-log-based velocity and density models for the Montney unconventional resource play in northeast British Columbia, Canada, applicable to induced seismicity monitoring and research. *Seismol. Res. Lett.* 92, 886–894.

Bao, X., Eaton, D.W., 2016. Fault activation by hydraulic fracturing in Western Canada. *Science* 354, 1406–1409.

Barclay, J., Krause, F., Campbell, R., Utting, J., 1990. Dynamic casting and growth faulting: Dawson Creek graben complex, Carboniferous–Permian Peace River embayment, Western Canada. *Bull. Can. Pet. Geol.* 38, 115–145.

Davies, G.R., Watson, N., Moslow, T.F., MacEachern, J.A., 2018. Regional subdivisions, sequences, correlations and facies relationships of the lower Triassic Montney formation, West-central Alberta to northeastern British Columbia, Canada – with emphasis on role of paleostructure. *Bull. Can. Pet. Geol.* 66, 23–92.

Deng, K., Liu, Y., Harrington, R.M., 2016. Poroelastic stress triggering of the December 2013 Crooked Lake, Alberta, induced seismicity sequence. *Geophys. Res. Lett.* 43, 8482–8491.

Dokht, R.M.H., Kao, H., Babaie Mahani, A., Visser, R., 2021. Spatiotemporal analysis of seismotectonic state of injection-induced seismicity clusters in the Western Canada sedimentary basin. *J. Geophys. Res., Solid Earth* 126, e2020JB021362.

Eaton, D.W., Ross, G.M., Hope, J., 1999. The rise and fall of a cratonic arch: a regional seismic perspective on the Peace River Arch, Alberta. *Bull. Can. Pet. Geol.* 47, 346–361.

Ellsworth, W.L., 2013. Injection-induced earthquakes. *Science* 341, 1225–1229.

Eyre, T.S., Eaton, D.W., Garagash, D.I., Zecevic, M., Venieri, M., Weir, R., Lawton, D.C., 2019. The role of aseismic slip in hydraulic fracturing-induced seismicity. *Sci. Adv.* 5, eaav7172.

Farahbod, A.M., Kao, H., Walker, D.M., Cassidy, J.F., Calvert, A., 2015. Investigation of regional seismicity before and after hydraulic fracturing in the Horn River Basin, northeast British Columbia. *Can. J. Earth Sci.* 52, 112–122.

Galloway, E., Hauck, T., Corlett, H., Paná, D., Schultz, R., 2018. Faults and associated karst collapse suggest conduits for fluid flow that influence hydraulic fracturing-induced seismicity. *Proc. Natl. Acad. Sci. USA* 115, E10003–E10012.

Gao, D., Kao, H., Wang, B., Visser, R., Schultz, R., Harrington, R.M., 2022. Complex 3D migration and delayed triggering of hydraulic fracturing-induced seismicity: a case study near Fox Creek, Alberta. *Geophys. Res. Lett.* 49, e2021GL093979.

Goebel, T., Weingarten, M., Chen, X., Haffener, J., Brodsky, E., 2017. The 2016 Mw5.1 Fairview, Oklahoma earthquakes: evidence for long-range poroelastic triggering at >40 km from fluid disposal wells. *Earth Planet. Sci. Lett.* 472, 50–61.

Healy, J.H., Rubey, W.W., Griggs, D.T., Raleigh, C.B., 1968. The Denver Earthquakes. *Science* 161, 1301–1310.

Ikari, M.J., Niemeijer, A.R., Spiers, C.J., Kopf, A.J., Saffer, D.M., 2013. Experimental evidence linking slip instability with seafloor lithology and topography at the Costa Rica convergent margin. *Geology* 41, 891–894.

Kao, H., Visser, R., Smith, B., Venables, S., 2018. Performance assessment of the induced seismicity traffic light protocol for northeastern British Columbia and Western Alberta. *Lead. Edge* 37, 117–126.

Keranen, K.M., Weingarten, M., 2018. Induced seismicity. *Annu. Rev. Earth Planet. Sci.* 46, 149–174.

Lei, X., Huang, D., Su, J., Jiang, G., Wang, X., Wang, H., Guo, X., Fu, H., 2017. Fault reactivation and earthquakes with magnitudes of up to Mw4.7 induced by shale-gas hydraulic fracturing in Sichuan basin, China. *Sci. Rep.* 7, 7971.

Lei, X., Wang, Z., Su, J., 2019. The December 2018 ML 5.7 and January 2019 ML 5.3 earthquakes in South Sichuan basin induced by shale gas hydraulic fracturing. *Seismol. Res. Lett.* 90, 1099–1110.

Mahani, A.B., Kao, H., Walker, D., Johnson, J., Salas, C., 2016. Performance evaluation of the regional seismograph network in northeast British Columbia, Canada, for monitoring of induced seismicity. *Seismol. Res. Lett.* 87, 648–660.

O'Connell, S., Mossop, G., Shetsen, I., 1994. Geological history of the Peace River Arch. In: Mossop, G.D., Shetsen, I. (Eds.), *Geological Atlas of the Western Canada Sedimentary Basin*. Canadian Society of Petroleum Geologists and Alberta Research Council.

Peña Castro, A.F., Roth, M.P., Verdecchia, A., Onwumeka, J., Liu, Y., Harrington, R.M., Zhang, Y., Kao, H., 2020. Stress Chatter via fluid flow and fault slip in a hydraulic fracturing-induced earthquake sequence in the Montney formation, British Columbia. *Geophys. Res. Lett.* 47, e2020GL087254.

Raleigh, C., Healy, J., Bredehoeft, J., 1976. An experiment in earthquake control at Rangely, Colorado. *Science* 191, 1230–1237.

Riazi, N., Eaton, D.W., 2020. Anatomy of a buried thrust belt activated during hydraulic fracturing. *Tectonophysics* 795, 228640.

Sanders, S., Etienne, C., Gogolick, A., Kelly, D., Zonneveld, J.-P., 2018. The Middle Montney Altares Member: lithology, depositional setting and significance for horizontal drilling and completion in the Altares Field, British Columbia. *Bull. Can. Pet. Geol.* 66, 318–337.

Savvaiddis, A., Lomax, A., Breton, C., 2020. Induced seismicity in the Delaware basin, West Texas, is caused by hydraulic fracturing and wastewater disposal. *Bull. Seismol. Soc. Am.* 110, 2225–2241.

Schultz, R., Atkinson, G., Eaton, D., Gu, Y., Kao, H., 2018. Hydraulic fracturing volume is associated with induced earthquake productivity in the Duvernay play. *Science* 359, 304–308.

Schultz, R., Corlett, H., Haug, K., Kocon, K., MacCormack, K., Stern, V., Shipman, T., 2016. Linking fossil reefs with earthquakes: geologic insight to where induced seismicity occurs in Alberta. *Geophys. Res. Lett.* 43, 2534–2542.

Schultz, R., Eaton, D.W., 2018. Increased likelihood of induced seismicity in highly overpressured shale formations. *Geophys. J. Int.* 214, 751–757.

Schultz, R., Wang, R., 2020. Newly emerging cases of hydraulic fracturing induced seismicity in the Duvernay East shale basin. *Tectonophysics* 779, 228393.

Segall, P., Lu, S., 2015. Injection-induced seismicity: poroelastic and earthquake nucleation effects. *J. Geophys. Res., Solid Earth* 120, 5082–5103.

Shen, L.W., Schmitt, D.R., Haug, K., 2019. Quantitative constraints to the complete state of stress from the combined borehole and focal mechanism inversions: Fox Creek, Alberta. *Tectonophysics* 764, 110–123.

Skoumal, R.J., Brudzinski, M.R., Currie, B.S., 2018. Proximity of Precambrian basement affects the likelihood of induced seismicity in the Appalachian, Illinois, and Williston Basins, central and eastern United States. *Geosphere* 14, 1365–1379.

Tan, F., Kao, H., Nissen, E., Eaton, D., 2019. Seismicity-scanning based on navigated automatic phase-picking. *J. Geophys. Res., Solid Earth* 124, 3802–3818.

Verberne, B., Spiers, C.J., Niemeijer, A.R., De Bresser, J., De Winter, D., Plümper, O., 2014. Frictional properties and microstructure of calcite-rich fault gouges sheared at sub-seismic sliding velocities. *Pure Appl. Geophys.* 171, 2617–2640.

Wang, B., Harrington, R.M., Liu, Y., Kao, H., Yu, H., 2020. A study on the largest hydraulic-fracturing-induced earthquake in Canada: observations and static stress-drop estimation. *Bull. Seismol. Soc. Am.* 110, 2283–2294.

Wang, B., Verdecchia, A., Kao, H., Harrington, R.M., Liu, Y., Yu, H., 2021. A study on the largest hydraulic fracturing induced earthquake in Canada: numerical modeling and triggering mechanism. *Bull. Seismol. Soc. Am.* 111 (3), 1392–1404.

- Wiemer, S., Wyss, M., 2000. Minimum magnitude of completeness in earthquake catalogs: examples from Alaska, the Western United States, and Japan. *Bull. Seismol. Soc. Am.* 90, 859–869.
- Yu, H., Harrington, R.M., Kao, H., Liu, Y., Abercrombie, R.E., Wang, B., 2020. Well proximity governing stress drop variation and seismic attenuation associated with hydraulic fracturing induced earthquakes. *J. Geophys. Res., Solid Earth* 125, e2020JB020103.
- Yu, H., Harrington, R.M., Kao, H., Liu, Y., Wang, B., 2021a. Fluid-injection-induced earthquakes characterized by hybrid-frequency waveforms manifest the transition from aseismic to seismic slip. *Nat. Commun.* 12, 6862.
- Yu, H., Harrington, R.M., Liu, Y., Wang, B., 2019. Induced seismicity driven by fluid diffusion revealed by a near-field hydraulic stimulation monitoring array in the Montney basin, British Columbia. *J. Geophys. Res., Solid Earth* 124, 4694–4709.
- Yu, H., Kao, H., Visser, R., Wang, B., 2021b. From seismic quiescence to surged activity after decades of wastewater disposal: a case study in central-West Alberta, Canada. *Geophys. Res. Lett.* 48, e2021GL095074.
- Yuan, J., Kao, H., Yu, J., 2020. Depth-scanning algorithm: accurate, automatic, and efficient determination of focal depths for local and regional earthquakes. *J. Geophys. Res., Solid Earth* 125, e2020JB019430.
- Zoback, M.D., Lund Snee, J.-E., 2018. Predicted and observed shear on pre-existing faults during hydraulic fracture stimulation. In: *SEG Technical Program Expanded Abstracts 2018*. Society of Exploration Geophysicists, pp. 3588–3592.
- Zonneveld, J.-P., Moslow, T.F., 2018. Palaeogeographic setting, lithostratigraphy, and sedimentary framework of the lower Triassic Montney formation of Western Alberta and northeastern British Columbia. *Bull. Can. Pet. Geol.* 66, 93–127.